Combinatorial prospects of nanoparticle mediated immunotherapy of cancer

Silva, C.G. da

6

COMBINING PHOTODYNAMIC THERAPY WITH IMMUNOSTIMULATORY NANOPARTICLES ELICITS EFFECTIVE ANTI-TUMOR IMMUNE RESPONSES IN PRECLINICAL MURINE MODELS

Huis in 't Veld, Ruben V*.; da Silva, Candido G.*; Jager, Martine J.; Cruz, Luis J.; Ossendorp, Ferry.

* Authors contributed equally to the study and share first authorship

Submitted for publication

Abstract

Photodynamic therapy (PDT) has shown encouraging but limited clinical efficacy when used as a standalone treatment against solid tumors. Conversely, a limitation for immunotherapeutic efficacy is related to the immunosuppressive state observed in large, advanced tumors. In the present study, we employ a strategy in which we use a combination of PDT and immunostimulatory nanoparticles (NPs), consisting of poly(lactic-co-glycolic) acid (PLGA)-polyethylene glycol (PEG) particles loaded with the Toll-like receptor 3 (TLR3) agonist poly(I:C), the TLR7/8 agonist R848, and the lymphocyte-attracting chemokine, macrophage inflammatory protein 3α (MIP3α). The combination provoked strong anti-tumor responses, including an abscopal effect, in three clinically relevant murine models of cancer: MC38 (colorectal), CT26 (colorectal) and TC-1 (human papillomavirus 16 induced). We show that the local and distal anti-tumor effects depended on the presence of CD8+ T cells. The combination elicited tumor-specific, oncoviral or neoepitope directed CD8+ T-cell immune responses against the respective tumors, providing evidence that PDT can be used as an in-situ vaccination strategy against cancer (neo)epitopes. Finally, we show that the treatment alters the tumor microenvironment in tumor-bearing mice, from cold (immunosuppressed) to hot (pro-inflammatory), based on greater neutrophil infiltration and higher levels of inflammatory myeloid and CD8+ T cells compared to untreated mice. Together, our results provide a rationale for combining PDT with immunostimulatory NPs for the treatment of solid tumors.

INTRODUCTION

Cancer treatment currently consists of various modalities and combinations thereof, including surgical resection, radiotherapy, chemotherapy, photodynamic therapy (PDT) and immunotherapy. Interestingly, PDT can potentially serve three purposes: firstly, it can kill cancer cells directly; secondly, it can induce damage to the tumor vasculature, depending on the photosensitizer and protocols used, that lead to an impaired vascular structure or complete vascular shutdown; and thirdly, it can trigger anti-cancer immune responses.1,2 Specifically, PDT functions by generating reactive oxygen species that subsequently damage cells in the tumor, its microenvironment and/or its vasculature. This type of photo-ablative damage to the tumor area can induce immunogenic cell death,3,4 initiating an immune response through the exposure and/or release of damage-associated molecular patterns (DAMPs) and, in some cases, cancer (neo)antigens.3 These DAMPs then activate diverse pattern-recognition receptors (PRRs) such as Receptor for Advanced Glycation End-products (RAGE), the Toll-like receptors (TLRs) TLR3/7/8/9, or Absent-in-Melanoma 2 (AIM2), among others, in dendritic cells (DCs), macrophages, epithelial and other cells. Several DAMPs have been shown to be highly important in the immune response following PDT, including high mobility group box 1 (HMBG1),5 surface-exposed calreticulin (CRT),4,6,7 the surface-exposed heat shock proteins HSP70 and HSP908–13, and extracellular ATP.14–16 Moreover, the curative effects of PDT strongly depend on the presence of a functional adaptive immune system.15 In this regard, we previously reported that depletion of CD8+ T cells before treatment abrogates the survival benefits of PDT.17

Cancer immunotherapy using immunostimulatory agents administered intratumorally, systemically or otherwise, has been investigated extensively. When administered intratumorally, such agents generally function by converting the tumor microenvironment and the tumor-draining lymph nodes (dLN) from an immunosuppressed (cold) to a pro-inflammatory (hot) state.18 We previously reported that intratumoral administration of the TLR3 ligand poly(I:C), the TLR7/8 ligand R848 and the chemokine MIP3α is effective in murine cancer models.19,20 Such TLR agonists are among the most potent of immunotherapies available and, accordingly, many of these agents are currently in clinical development.21 Similarly,

Polyinosinic:polycytidylic acid (poly(I:C), an analog of double-stranded RNA (dsRNA) and a potent agonist of the dsRNA-sensor TLR322, has been reported to inhibit the growth of certain tumors by converting them from immunologically cold to hot23–25 and to indirectly facilitate adaptive anti-tumor immune responses through the induction of the innate immune system.26 Additionally, poly(I:C) may also directly affect tumor cells by initiating cell death pathways via activation of caspase 8.27–30 Analogously, R848, an imidazoquinolinone derivative and agonist of the single-stranded-RNA (ssRNA)-sensor TLR7/8, induces immune responses based on signaling through MyD88 and NF-κB.31 It induces anti-tumor responses32, decreases the number of myeloid-derived suppressor cells (MDSCs) in tumors and promotes the conversion of MDSCs towards a more-mature antigen-presenting phenotype.33 Moreover, R848 has been reported to promote the polarization of tumor-associated macrophages to an M1-like phenotype, contributing to inhibition of tumor growth.34 Similarly, TLR8 signaling has been shown to reverse suppression and inhibit the generation of senescent tumor-specific T cells and of naïve T cells.35 Interestingly, R848 was shown to increase the expression of HMGB1, indicating synergistic potential for combination with PDT.32 Lastly, the chemokine MIP3α (CCL20) is a strong chemoattractant for lymphocytes36, and acts by binding to the chemokine receptor CCR6.37,38

To reduce the risk of adverse systemic immune events in patients, we aim to minimize diffusion of immunostimulatory agents from the tumor area. In this context, biocompatible nanoparticles (NPs) that can release drugs in a slow and sustained fashion are ideal vehicles for intratumoral delivery of such agents39, offering clear advantages over free (nude) drugs.40 Specifically, poly(lactic-co-glycolic) acid (PLGA) NPs and liposomes are both FDA-approved vehicles and already used in the clinic.41,42 Recently, we have reported that in mice, PLGA-based NPs can accumulate strongly in PDT-treated tumors compared to untreated tumors after systemic administration, providing a rationale for the combination of PDT and NP-based anti-tumor therapy.43 Here, we report a study in which PDT combined with intratumoral administration of PLGA NPs loaded with poly(I:C), R848 as well as MIP3α was analyzed for its therapeutic efficacy compared to either modality alone, in three murine cancer models: MC38 (colon adenocarcinoma model), CT26 (colon cancer carcinoma) and TC-1 (lung epithelial tumor expressing human papillomavirus (HPV)16 E6 and E7 oncoproteins). Of relevance, each of these murine models represents a human tumor that could be potentially treated

intratumorally in patients via fiber optics.44,45 In all three models, the combination treatment was highly efficacious. We observed strong anti-cancer immune responses with tumor (neo)antigen specific CD8+ T cells and an abscopal effect to a secondary tumor in the opposite flank. Finally, we found that our treatment modulated the immunosuppressive microenvironment into a more proinflammatory state. Together, our results indicate that a combination of PDT and intratumorally-administered PLGA NPs loaded with immunostimulatory agents elicits strong local and systemic anti-tumor immune responses in clinically relevant murine models of solid tumors.

MATERIALS AND METHODS

2.1 Materials and reagents

PLGA (Resomer RG 502 H, lactide:glycolide molar ratio 48:52 to 52:48) was purchased from Boehringer Ingelheim, Germany. Solvents used for PLGA preparation were obtained from Sigma-Aldrich (The Netherlands). The lipids were purchased from Avanti Polar Lipids (USA) and included 1,2-distearoyl-sn-glycero-3-phosphoethanolamine-N-[amine (polyethylene glycol)2000] (ammonium salt) and 1,2-distearoyl-sn-glycero-3-phosphoethanolamine-N-[methoxy(polyethylene glycol)-2000] (ammonium salt) (mPEG 2000 PE). Poly (inosinic:cytidylic acid (poly(I:C)) and the near-infrared (NIR) dye IR-780 were purchased from Sigma-Aldrich (Zwijndrecht, The Netherlands), R848 was obtained from Alexis Biochemicals (Paris, France) and MIP3α (CCL20) was purchased from R&D Systems (USA).

2.2 Preparation of PLGA-NPs

Poly-lactic-co-glycolic-acid-based NPs that encapsulate poly(I:C), R848 and MIP3α were prepared using an oil/water emulsion and the solvent evaporation-extraction method.46–49 In brief, 200 mg of PLGA was dissolved in 3 mL of dichloromethane (DCM), containing 8 mg of poly(I:C), 4 mg of R848 and 250 μg of MIP3α in addition to 1 mg of the NIR dye IR-780 when used for microscopy, and added drop-wise to 40 mL of aqueous 2.5 % (w/v) PVA in distilled water before emulsification for 120 sec using a sonicator (250W Sonifier 250, Branson, USA). After the DCM had been removed through air-drying, the lipid mPEG 2000 PE (20 mg) was dissolved in DCM and used to form a film layer on the bottom of a beaker. Subsequently, the emulsion was rapidly added to the beaker containing the lipids

and the solution was homogenized for 30 sec by sonification. Following overnight evaporation of the solvent at 4 °C, the PLGA NPs were collected by centrifugation at 25000 g for 10 min, washed four times with distilled water, and lyophilized. The concentration of the agents entrapped by the NPs was determined by reverse phase high-performance liquid chromatography and regression analysis, as described previously.19,50

2.3 Size distribution and surface charge of the NPs

The average size and zeta-potential of PLGA NPs was determined using a Zetasizer Nano ZSP (Malvern Panalytical, Malvern, UK). In brief, 50 µg of NP was dissolved in 1 mL MilliQ H2O after which the size was determined by dynamic light scattering and the surface charge was measured by laser Doppler electrophoresis.

2.4 Cell lines

The tumor cell line Murine Colon 38 (MC38) cells on C57BL/6 background and the murine colon carcinoma cell line CT26 on BALB/c background were kindly provided by Mario Colombo and used for experiments without modification. The murine tumor cell line TC-1, expressing HPV16 E6 and E7 oncoproteins and the activated human c-Ha-ras oncogene, generated by retroviral transduction of lung fibroblasts obtained from C57BL/6 mice, was a gift from T.C. Wu (John Hopkins University, Baltimore, MD).51 The D1 dendritic cell (D1DCs) line, an immature splenic dendritic cell (DC) that resembles bone marrow-derived DCs52, was cultured as described previously.53 All cells used were tested for mycoplasma and were MAP tested before the onset of experiments. All tumor cell lines were cultured in culture medium, consisting of Iscove's Modified Dulbecco's Medium (IMDM, Lonza, Basel, Switzerland) supplemented with 8% Fetal Calf Serum (Greiner, Kremsmünster, Austria), 2 mM glutamine (Gibco, Landsmeer, The Netherlands), 100 IU/mL penicillin/streptomycin (Gibco) and 25 µM 2-mercaptoethanol (Sigma-Aldrich) and kept in an incubator (Panasonic) at 37 °C and 5% CO2. For TC-1, the culture medium was further supplemented with 400 µg/mL of the selection antibiotic Geneticin (G418; Life Technologies).

2.5 Animal models

All animal experiments were performed in accordance with the Code of Practice of the Dutch Animal Ethical Commission. Female BALB/c mice (6 to 12 weeks old) were purchased from Charles River (Ecully, France) and C57BL/6J mice were purchased from ENVIGO (Horst, the Netherlands). The animals were housed in the animal facility of the LUMC under specified pathogen-free conditions.

2.6 Photosensitizer uptake and retention experiments

Photosensitizer uptake and retention were evaluated by seeding 4 x 10^4 MC38, 3 x 10^4 CT26 or 2.5 x 10^4 TC-1 cells in separate wells of a 24-well plate (Corning, Glendale, USA) in culture medium and subsequent incubation overnight at 37 ºC and 5 % CO2. For the uptake experiments, cells were incubated with indicated concentrations of Radachlorin® (Radapharma International, Loon op Zand, The Netherlands) for a specified time. Following incubation, the cells were washed 3 times with PBS and fixed in Phosphate Buffered Saline (PBS) containing 1% formalin (J.T. Baker) at 4 ºC for 15 min. The fixative was then washed away with PBS, after which the cells were reconstituted in Fluorescence-Activated Cell Sorting (FACS) buffer (PBS with 0.5 % Bovine Serum Albumin (BSA) and 0.02 % sodium azide). The fluorescence of the photosensitizer was used to determine its uptake using flow cytometry on an LSR II (BD Biosciences, San Jose, USA). For the retention experiment, cells incubated with photosensitizer for 4 h were washed 3 times in PBS and supplied with fresh culture medium. After an indicated amount of time, the samples were washed 3 times in PBS, fixed in 1% formalin at 4 ºC for 15 min before washing in PBS, reconstituting in FACS buffer and analysis by flow cytometry.

2.7 PDT in vitro cytotoxicity

For PDT in vitro, 4 x 10^4 MC38, 3 x 10^4 CT26 and 2.5 x 10^4 TC-1 cells were seeded in 24-well plates (Corning) in culture medium and kept overnight at 37 ºC and 5% CO2. Cells were then incubated with 2 µM Radachlorin®, unless indicated otherwise, for a specified amount of time, washed 3 times with PBS and supplied with 500 µl fresh medium. Illumination was performed at a light intensity (fluence rate) of 116 mW/cm2 for a total light dose (fluence) of 20 J/cm2 using a 662 nm Milon Lakhta Laser, unless indicated otherwise. The following day, the cells were collected in FACS buffer, stained with Annexin V-FITC (BD Biosciences) at 3 µL per sample and 0.5 µM 4′,6-diamidino-2-phenylindole (DAPI) (Sigma-Aldrich) in

Annexin V binding buffer (0.1 M 4-(2-hydroxyethyl)-1-piperazineethanesulfonic acid (HEPES), 1.4 M NaCl, and 25 mM CaCl2 in deionized water with a pH set to 7.4. sterile filtered using a 0.2 µm filter), and finally, analyzed by flow cytometry. As a positive control, cells were subjected to three freeze/thaw cycles at -20 ºC before staining and analysis by flow cytometry.

2.8 Maturation of D1DCs after incubation with NPs

The biological activity of the NP-encapsulated agents was evaluated by seeding 5×10^4 D1DCs in 96-well plates (Corning) and incubating them with the NPs for 48 h in an incubator. The NP concentrations were matched to poly(I:C) at 5 µg/mL and serially diluted according to annotated concentrations to establish a dose-response curve, to enable comparison with the free ligand at 5 µg/mL. The cells were stained for the DC maturation markers CD86 and CD40 using anti-CD86-APC (clone GL1, eBioscience, Waltham, USA) and anti-CD40-PE (clone 1C10, eBioscience), respectively, and expression was measured by flow cytometry. The supernatant was collected after which IL12 was analyzed by a standard sandwich ELISA using the purified anti-mouse IL12/IL23 p40 (clone C15.6, Biolegend, San Diego, USA) and biotin-labelled anti-mouse IL12/IL23p40 antibodies (clone C17.8, Biolegend). The plates were read at 450 nm using a Bio-Rad 680 microplate reader (Bio-Rad Laboratories, Veenendaal, The Netherlands).

2.9 Toxicity of the NPs

The toxicity of the NPs to MC38, CT26 and TC-1 cells was determined by seeding 5×10^4 cells in 96-well plates (Corning) and incubating them with the NPs in a range of concentrations (6.25 µg/mL to 200 µg/mL) for 72 h. Cell viability was measured by adding 3-(4,5-dimethylthiazol-2-yl)-5-(3-carboxymethoxyphenyl)-2-(4-sulfophenyl)-2H-tetrazolium (MTS) reagent according to manufacturer instructions (Abcam, Cambridge, UK), and absorption was measured at 490 nm on a Bio-Rad iMark microplate absorbance reader after incubation.

2.10 Maturation of D1DCs after incubation with PDT-treated tumor cells

The immunostimulatory effects of PDT were preliminarily ascertained in a cellular assay involving dying PDT-treated cells and D1 dendritic cells. Firstly, 10^4 D1DCs were seeded in 96-well plates (Corning) for 24h. The following day, tumor cells were incubated with 2 µM Radachlorin® for 4 h (as described in 2.7), and then treated with PDT at 116 mW/cm2 for 20 J/cm2. These (dying) treated tumor cells were

then added to the D1DCs at a ratio of 20:1 (tumor cell/D1DC), and the cells were incubated together for a further 24 h in an incubator. The cells were then collected, stained with 0.5 μM DAPI (Sigma-Aldrich), CD11c-APC-Cy7 (clone N418 Thermo Fisher Scientific, Waltham, USA), MHC-II-PE (H-2kb AF6-88.5, BD Biosciences) and CD86-FITC (clone GL1, eBioscience), and finally, analyzed by flow cytometry on an LSR-II (BD Biosciences). Live D1DCs were gated based on DAPI-CD11chi after size/morphology and doublet exclusion based on FSC/SCC patterns.

2.11 PDT and NP tumor treatments in vivo

For PDT in vivo, C57BL/6J mice were inoculated with 0.5 x 10^6 MC38 or 1 x 10^5 TC-1 cells in 200 μL PBS and BALB/c mice were inoculated with 0.2 x 10^6 CT26 cells in 200 μL PBS, on the left and/or right flanks as indicated per experiment. Once the tumors had reached an average volume of approximately 125 mm3, the mice were randomly divided into groups and treated with PDT as described previously.17,54 Briefly, 20 mg/kg Radachlorin® was administered intravenously into the tail vein and allowed to distribute for 6 h. Then, the skin surrounding the tumor area was shaved before illumination under isoflurane anesthesia at a fluence rate of 116 mW/cm2 over 1000 sec for a fluence of 116 J/cm2. The next day, the mice were injected intratumorally with NPs at concentrations corresponding to 2.5 mg/kg (50 μg) poly(I:C), at 0.7 mg/kg (14 μg) of R848 and 0.05 mg/kg (1 μg) of MIP3α in a total volume of 30 μL per treatment. These intratumoral injections were repeated every other day for a total of four treatments for the MC38 and CT26 models, and a total of two treatments for the TC-1 model. From this point onwards, the tumor growth was measured regularly until the end of the experiment.

2.12 Detection of blood tetramers

The capacity of PDT and the NPs to induce antigen-specific T cells in the blood of TC-1 tumor-bearing mice were determined analyzing (25 μL) blood obtained from the tail vein at day 8 after PDT. Red blood cells were removed using lysis buffer after which the cells were incubated with an APC labeled, MHC class I (H-2Db) HPV16 E749-57 (RAHYNIVTF) (H-2Db) tetramer. Next, the cells were stained with anti-CD8α-PE (clone 53-6.7, eBioscience), anti-CD3-eFluor 450 (clone 17A2, eBioscience) and analyzed by flow cytometry on an LSR-II (BD Biosciences). Gating of CD8+ T cells was based on CD3+CD8+ events after size/morphology and doublet exclusion based on FSC/SCC patterns.

2.13 Depletion of CD8+ cells

Mice were treated with 1 mg/kg (20 µg) anti-CD8-depleting antibodies via subcutaneous injection (clone 2.43) in 100 µL PBS every 7 days, starting one day before treatment. Circulating CD8+ T cells were qualified by analyzing blood (50 µL) obtained from the tail vein the morning before treatment. Red blood cells were removed using lysis buffer after which the cells were stained with anti-CD8α-PE (clone 53-6.7, eBioscience), and then anti-CD3-eFluor 450 (clone 17A2, eBioscience) analyzed by flow cytometry on an LSR-II (BD Biosciences).

2.14 Analysis of the tumor microenvironment, draining lymph node and spleen

Immunocompetent mice were inoculated with tumor cells in the right and left flanks, and then subcutaneously injected with CD8-depleting antibodies one day before tumors became established. When the tumors were established (~125mm3), PDT was performed on one tumor by administration of 20 mg/kg Radachlorin in the tail vein and irradiating with 662 nm light at a drug-to-light interval of 6 h at 116 mW/cm2 for 116 J/cm2. The next morning, animals were intratumorally injected with the NPs at an interval of 2 days. The day following the second NP administration, the mice were sacrificed after which the tumors, tumor-draining lymph node of the treated tumor and the spleen were harvested, processed and stained for analysis by flow cytometry. Tumors were excised, and then incubated with Liberase protease mix (Sigma) for 15 min to 30 min at 37°C. Liberase-treated tumor fragments, spleens and lymph nodes were processed through a cell strainer (Corning) to obtain single-cell suspensions. The samples were washed 2 times with culture medium and then washed 2 times with FACS buffer. Samples were stained with antibody mixes (see below) for analysis by flow cytometry. All flow cytometric analyses were performed on samples provided in FACS buffer on a Cytek Aurora 5-Laser flow cytometer (Cytek, Fremont, USA). The myeloid antibody panel consisted of CD11b-eFluor450 (clone M1/70 Thermo Fisher), Ly6C-BV605 (clone HK1.4 Biolegend), F4/80-FITC (clone BM8 Biolegend), Ly6G-AF700 (clone 1A8 Biolegend), CD45.2-APC-eFluor780 (clone 104 Thermo Fisher) and 7AAD (Invitrogen) viability staining. The lymphoid antibody panel consisted of CD44-V450 (IM7 Thermo Fisher), CD3e-FITC (Clone 145-2C11 Thermo Fisher), CD4-APC (clone RM4-5 Thermo Fisher), CD8α-APC-R700 (clone 53-6.7 BD Biosciences), CD45.2-APCeFluor780 (clone 104 Thermo Fisher) and 7AAD viability staining (Invitrogen).

2.15 Intracellular cytokine staining

Single-cell suspensions of splenocytes obtained as in 2.14 were incubated with D1DCs that were loaded overnight with 5 µM synthetic peptides of the MC38 neoepitopes Adpgk (peptide sequence: HLELASMTNMELMSSIVHQ) and Rpl18 (peptide sequence: KAGGKILTFDRLALESPK)55,56, in presence of 2 µg/mL Brefeldin A for 8h at 37°C. The samples were then stained with antibody mixes for flow cytometry. Again, all cytometric analyses were performed on samples provided in FACS buffer on a Cytek Aurora 5-Laser flow cytometer. The antibody panel consisted of Granzyme B-V450 (clone NGZB Thermo Fisher), CD3-BV510 (clone 145-2C11 BD Biosciences), TNFα-FITC (clone MP6-XT22 Thermo Fisher), IL-2-PE (clone JES6-5H4 Thermo Fisher), IFN-γ-PE-Cy7 (clone XMG1.2 BD Biosciences), CD8α-APC-R700 (clone 53-6.7 BD Biosciences) and 7AAD viability staining (Invitrogen).

2.16 Statistics

Graph Pad Prism software version 8 was used for statistical analysis. Data were analyzed as indicated for individual experiments.

RESULTS

PDT in vitro

We previously studied and characterized PDT with the photosensitizer (PS) Radachlorin, reporting strong induction of anti-tumor responses and disruption of the tumor vasculature in the MC38 tumor model.43 In the current study, we used flow cytometry to show that Radachlorin is internalized by MC38, CT26 and TC-1 cells over time, with uptake increasing up to 8 h post-incubation (Figure 1A). Binding of the PS, as investigated by incubation at 4 ºC, induces a markedly lower fluorescent signal when compared to the uptake in all three tested cell lines over time (Figure 1A), indicating that the majority of the PS is indeed taken up by the cells. Furthermore, the PS was shown to stay inside the cells up to at least 6h post-pulse (Figure 1B). Moreover, we confirmed that Radachlorin was non-toxic to all the tested cell lines after incubation, in the absence of light (dark toxicity), at Radachlorin concentrations from 0.1 μM to 100 μM (Figure 1C). We investigated the effect of in vitro PDT on cell viability after 4 h of incubation at 2 μM Radachlorin, followed by illumination with 662 nm laser light at a fluence rate of 116mW/cm2 for a fluence of 20 J/cm2. Flow cytometry based on staining for the death marker DAPI and early apoptotic marker Annexin V (Figure 1D) was subsequently applied on the treated cells. The single PDT treatment induced near-complete cell death, comparable to three freeze/thaw cycles at -20 ºC. Importantly, at 2 J/cm2, approximately 61±4% of MC-38, 49±3% of CT26 and 23±6% of TC-1 cells were stained by Annexin V and/or DAPI, indicating differences in sensitivity to PDT among tumor cell lines. PDT-induced cell death diminished with decreasing fluence: at a fluence of 0.2 J/cm2, we observed levels of cell death comparable to those in the untreated tumor cells. Together, our results indicate that the photosensitizer Radachlorin is gradually internalized by MC38, CT26 and TC-1 tumor cells in vitro; that it remains in these cells for up to 6 h post-incubation; that it does not exhibit dark toxicity; and that, following PDT, it kills cells from all three tumor lines at levels similar those obtained by multiple freeze/thaw cycles.

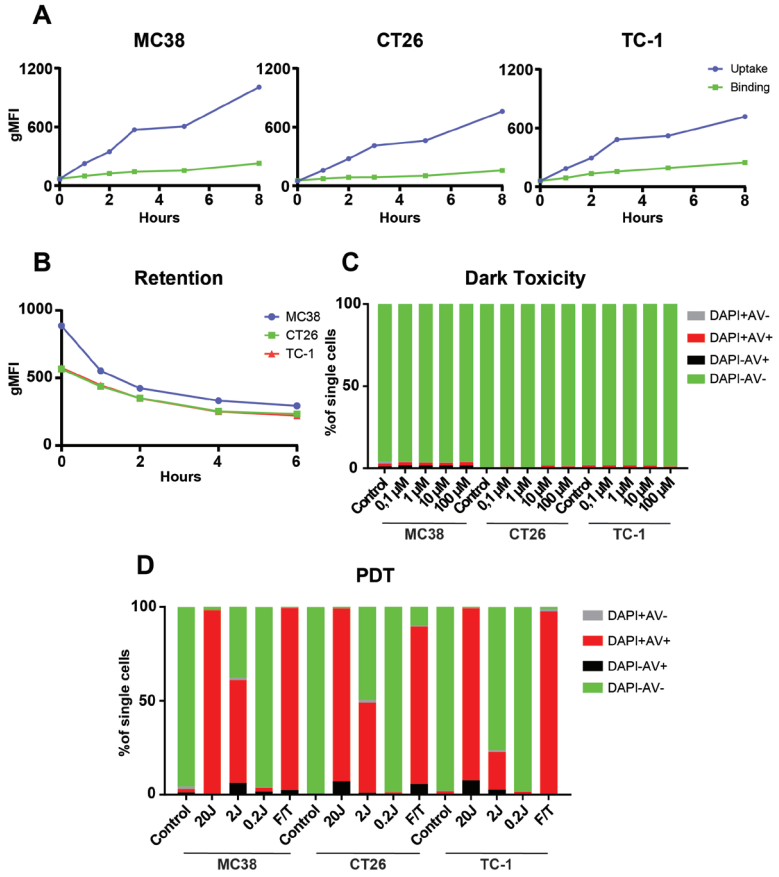

Figure 1. Cellular uptake, binding, retention and cytotoxicity of the photosensitizer Radachlorin in three clinically relevant tumor cell lines

A). Cellular uptake and binding assays with the photosensitizer Radachlorin (2 µM) in MC38, CT26 and TC-1 cells over time. The uptake and binding assays were performed by incubating cells with photosensitizer at 37 °C and 4 °C, respectively. Detection was performed by flow cytometry using the fluorescence of Radachlorin. **B)**. Retention of Radachlorin (2 µM) in MC38, CT26 and TC-1 cells after a pulse of 4 h, washing and detection by flow cytometry. **C)**. Dark toxicity after incubation with Radachlorin (0.1 µM to 100 µM) for 4 h, followed by washing and incubation overnight. Cells were stained with DAPI and Annexin V-FITC to determine cell viability by flow cytometry. D). Cytotoxicity of Radachlorin (2 µM) treatment

followed by PDT. Cells were incubated for 4 h, after which they were washed and irradiated with 662nm light 116 mW/cm2 (0.2 J/cm2 to 20 J/cm2). Three freeze/thaw cycles at -20 °C were used as positive control. The next day, the cells were stained with DAPI and Annexin V-FITC to determine their viability by flow cytometry.

Radachlorin PDT induces immunogenic cell death

Next, we investigated the immunological effects of PDT-induced cancer cell death on the maturation of dendritic cells (DCs). To this end, DCs were incubated for 24 h with PDT-treated cancer cells and evaluated for expression of the maturation markers CD86 and MHC-II by flow cytometry. For MC38 cells, the protocol that induced the strongest cell death also induced the greatest upregulation of both markers at levels higher than those observed for the positive control, three freeze/thaw cycles (Figure 2A). Moreover, the PDT-treated cancer cells induced upregulation of the maturation markers at levels comparable to treatment with 1 μg/mL of the TLR3 ligand poly(I:C), an immunostimulatory agent that induces strong upregulation of these markers. A similar trend was observed for CT26, although the upregulation of the markers was lower than for MC38 (Figure 2B). Finally, incubation of the DCs with TC-1 cancer cells induced a slight upregulation of the maturation markers, with levels only slightly increased compared to incubation with the positive control of three freeze/thaw cycles (Figure 2C). Taken together, these results suggest that PDT treatment of MC38 and CT26 cells, and to a much smaller extent of TC-1 cells, leads to strong upregulation of maturation markers on DCs in vitro.

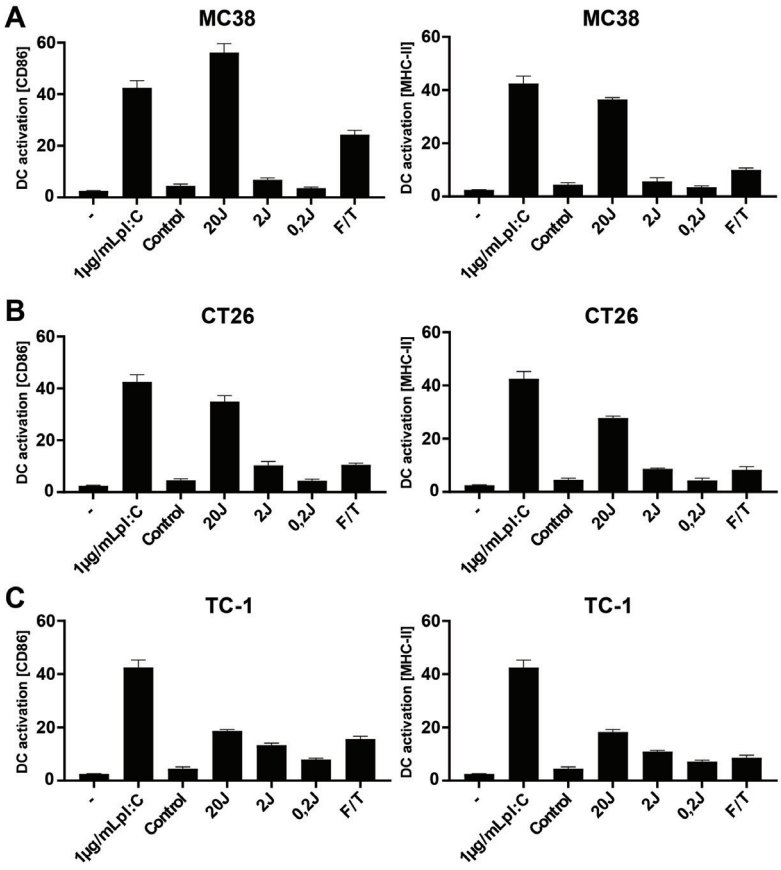

Figure 2. Immune stimulating effects of PDT-induced cancer cell death on dendritic cells MC38 (A), CT26 (B) or TC-1 (C) cells were treated by PDT after 4 h of incubation with Radachlorin (2 µM) at 116 mW/cm2 (0.2 J/cm2 to 20 J/cm2) or three freeze/thaw (F/T) cycles at -20 ºC, incubated with murine DCs for 24 h immediately post-treatment. The percentage of CD86hi and MHC-IIhi cells in live DCs (CD11c+DAPI- cells) were compared to untreated DCs (-), to DCs incubated with poly(I:C) (1 µg/mL), and to DCs incubated with untreated MC38 (control). Data from three independent assays shown as a mean ± SD.

Physicochemical characterization and biological activity of PLGA-PEG (poly(I:C), R848, MIP3α) NPs

We previously characterized the PLGA-based NPs that we used in this study for the local, slow and sustained release of poly(I:C), R848 and MIP3α for size, zeta-potential, TEM morphology, stability, drug release kinetics, uptake, cytotoxicity, DC maturation and chemoattractant capacity.19 Moreover, we reported in another study on the immunological effects of NP-encapsulated poly(I:C), R848 and of MIP3α, either combined or separate, in MC38 and TC-1 models.20 For the current study, we re-analyzed an aliquot of NPs from the pooled production batches. The NPs exhibited an average size of 249.6 nm, as evaluated by dynamic light scattering (Figure S1A and Table 1) and an average zeta-potential (ζ) potential of -21.4mV, as determined using a Zetasizer (Figure S1B and Table 1).

Table 1. Physicochemical characterization of the NPs

Sample	Diameter	ζ Potential	PDI	Loading capacity (% w/w)			
				NIR	poly(I:C)	R848	MIP3α
NP (NIR+pIC+R848+ MIP3α) -PEG	249.6 ± 85.4	-21.4 ± 4.75	0.178	62.4 ± 6.9	43.6 ± 8.6	54.2 ± 8.9	59.3 ± 7.3

Physicochemical characterization of the PLGA-PEG NPs containing immunostimulatory agents. The PLGA NPs were characterized by dynamic light scattering and zeta potential measurements. The size and zeta potential data represent the mean value ± SD of 10 readings of one representative batch. The loading capacity of the NIR dye was measured by fluorescence. The loading capacity of poly(I:C), R848 and MIP3α was determined by RP-HPLC analysis.

To determine whether the biological activity of the encapsulated compounds had been preserved during NP synthesis and storage, we incubated the NPs with DCs in a range of concentrations (0 μg/mL to 5 μg/mL poly(I:C)). The expression of the maturation markers CD40 and CD86 was evaluated after incubation with the NPs:

both maturation markers were upregulated at levels comparable to that observed for treatment with free (nude) poly(I:C) added at equimolar concentration (Figure S1C), indicating that the encapsulated compounds had retained their biological activity. Further corroborating the immunostimulatory activity of their cargo, the NPs also induced production of IL-12 at similar levels to that observed for the treatment with free poly(I:C) (Figure S1D). The toxicity of the NPs was evaluated by MTS assay, after incubation at concentrations of 0 μg/mL to 200 μg/mL. The NPs did not exhibit any direct cytotoxicity to MC38 (Figure S1E), CT26 (S1F) or TC-1 (Figure S1G) cells, even at the highest concentration tested. Together, these results suggest that the NPs have favorable size and charge distributions, retain the immunostimulatory activity of their cargo and are non-toxic to tumor cells.

The combination of PDT and immunostimulatory NPs strongly inhibits tumor growth and induces anti-tumor immune responses in vivo

Next, we assessed the tumor-debulking capacity of PDT and the immunostimulatory effects of the NPs separately and combined in mice bearing MC38, CT26 or TC-1 tumors. Thus, mice with established tumors (average volume: ~125mm3) were treated with PDT after a drug-to-light interval of 6 h with 662nm light at a fluence rate of 116 mW/cm2 for a fluence of 116 J/cm2 (Figure 3A). The debulking effects of this PDT treatment on the tumor mass were pronounced in all three models, although the duration of the delay in tumor growth varied. Whereas the PDT treatment eradicated all MC38 tumors (Figure 3B), approximately half of the CT26 tumors resumed growth at a slow rate after 10 days (Figure 3C), while all the TC-1 tumors resumed growth after 10 days (Figure 3D). Treatment with intratumoral injections of NPs with the three immunostimulatory agents induced strong anti-tumor responses in the MC38 and CT26 models (Figure 3B and 3C); however, it showed little effect on the TC-1 model (Figure 3D). The combination of PDT and the NPs was as effective as PDT alone and as NPs alone in the MC38 model, as both treatments alone induced near-complete cures (Figure 3B); however, the combination showed superior efficacy to either treatment alone in the CT26 model, as the tumors remained in regression 10 days after co-treatment and induced an enhanced survival rate up to 70 days post treatment (Figure 3C). Furthermore, the combination treatment significantly delayed tumor growth in the TC-1 model, initially similar to PDT alone; however, the TC-1 tumor growth developed at a much slower

rate three weeks after the co-treatment than did those treated with PDT alone (Figure 3D). In cancer immunotherapy, CD8+ T cells are often central in successful tumor clearance. Therefore, we investigated the importance of this population in our setting by administering CD8-depleting antibodies starting one day before PDT treatment, and subsequently administering them periodically for the remainder of the experiment. For mice bearing MC38 or CT26 tumors, pre-treatment depletion of their CD8+ cells (Figures S2A and S2B) led to rapid tumor growth after an initial delay in growth that had directly followed treatment. Together, the above results demonstrate that the combination of PDT and immunostimulatory NPs in tumor-bearing mice induces strong, CD8-dependent anti-tumor immune responses with near-complete survival of MC38, strongly enhanced survival of CT26 and a delay in growth of TC-1 tumors.

Figure 3. Anti-tumor efficacy of PDT combined with immunostimulatory NPs in mice bearing MC38, CT26 or TC-1 tumors. >

A). Description of the protocol: immunocompetent mice were inoculated with tumor cells in the right flank (n≥10 mice per group). CD8-depleting antibodies were injected 1 day before treatment. Once the tumors had become established (~125mm3), the mice were treated with PDT by administering Radachlorin (20 mg/kg) via a tail-vein injection, followed by irradiation (662 nm) at a drug/light interval of 6 h, at 116 mW/cm2 for 116 J/cm2. The next morning, treatment with NPs was started with an interval of 2 days for a total of four (MC38 and CT26) or two (TC-1) i.t. administrations. B). Tumor-growth and survival curves for C57BL/6J mice bearing MC38 tumors. C). Tumor-growth and survival curves for BALB/c mice bearing CT26 tumors. D). Tumor-growth and survival curves for C57BL/6J mice bearing TC-1 tumors. Statistical analysis was done using the Students t-test, by comparing experimental groups at the indicated timepoints (*p<0.05, **p<0.01 and ***p<0.0001).

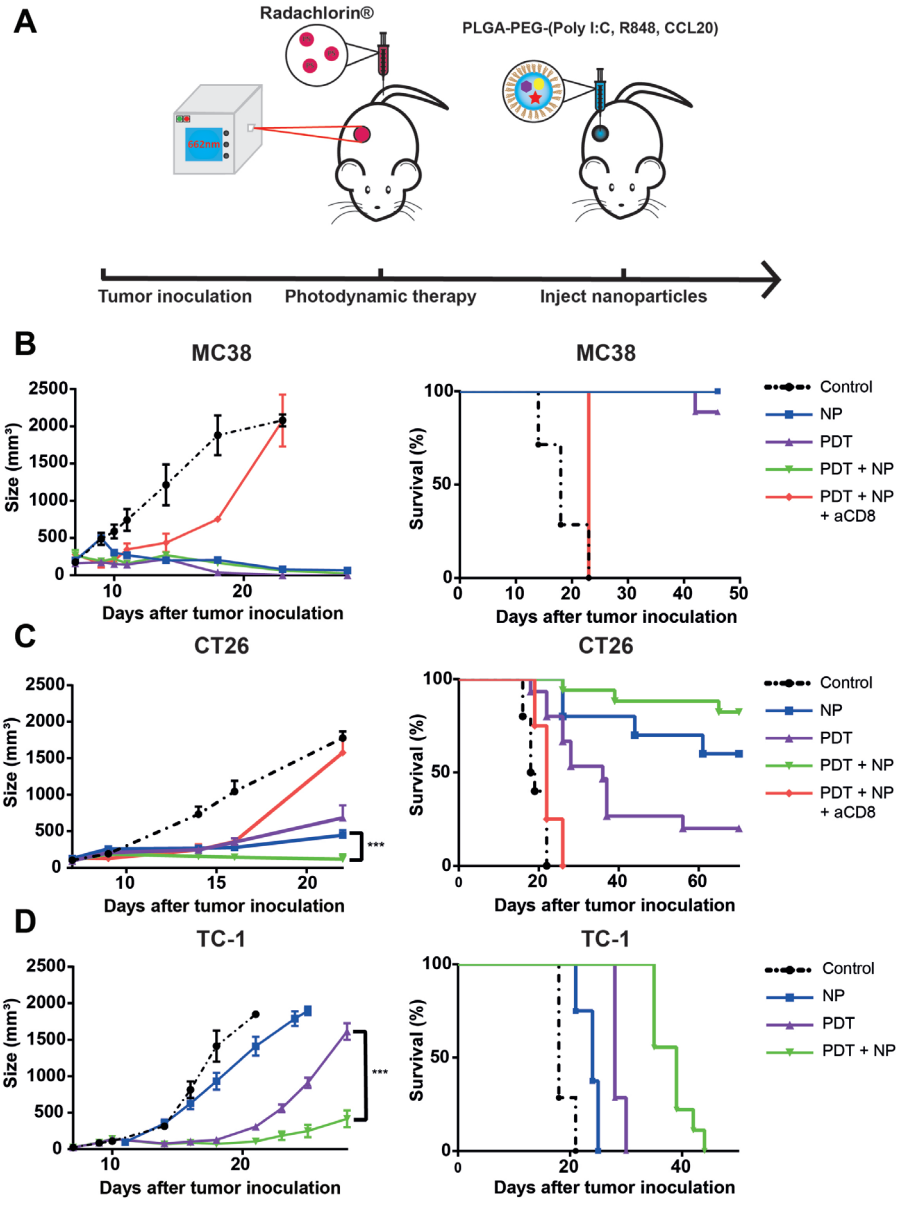
A
Radachlorin®
PLGA-PEG-(Poly I:C, R848, CCL20)
662nm
Tumor inoculation
Photodynamic therapy
Inject nanoparticles
B
MC38
Size (mm³)
Days after tumor inoculation
MC38
Survival (%)
Days after tumor inoculation
Control
NP
PDT
PDT + NP
PDT + NP + aCD8
C
CT26
Size (mm³)
Days after tumor inoculation
***
CT26
Survival (%)
Days after tumor inoculation
Control
NP
PDT
PDT + NP
PDT + NP + aCD8
D
TC-1
Size (mm³)
Days after tumor inoculation
***
TC-1
Survival (%)
Days after tumor inoculation
Control
NP
PDT
PDT + NP

The combination of PDT and NP elicits a CD8+ T-cell dependent abscopal effect in mice bearing bilateral MC38 or CT26 tumors

To study the induction of an abscopal effect by the treatments in the MC38 and CT26 models, we inoculated mice with two tumors, one on each opposing flank, and then treated only one of the tumors using the same protocol as above for mice bearing a single tumor (Figure 4A). For MC38, both the separate and combination treatment induced a delay in tumor growth on the untreated tumors compared to the control (untreated) mice, with the NP treatment and the combination treatment showing the strongest effects (Figure 4B). At 14 days post-inoculation, the combination induced an enhanced tumor growth inhibition on the total tumor burden compared to either treatment alone (Figure 4B), consequently extending the survival compared to PDT alone or control (untreated), but not versus NP alone (Figure S3A). A similar tumor growth delay was observed for the CT26 model (Figure 4C). As in MC38, in CT26 the NP treatment and the combination treatment induced the greatest effect, whereby PDT and the combination treatment induced the strongest effects on the treated tumors (Figure 4C). The combination treatment induced an enhanced tumor growth inhibition on the total tumor burden, when compared to PDT or NP alone (Figure 4C); however, as in MC38, it only provided superior survival relative to the control (untreated) (Figure S3B). Importantly and consistent with our previous results from the single-tumor experiments, CD8+ T cells were essential for greater survival of the treated groups: thus, in mice bearing bilateral MC38 (Figure 4A) or CT26 (Figure 4C) tumors, the benefits of the combination treatment on survival are completely abrogated after depletion of CD8+ T cells. Together, these results show that the combination of PDT and immunostimulatory NPs provides superior systemic anti-tumor immune responses in mice bearing bilateral MC38 or CT26 tumors compared to either treatment alone.

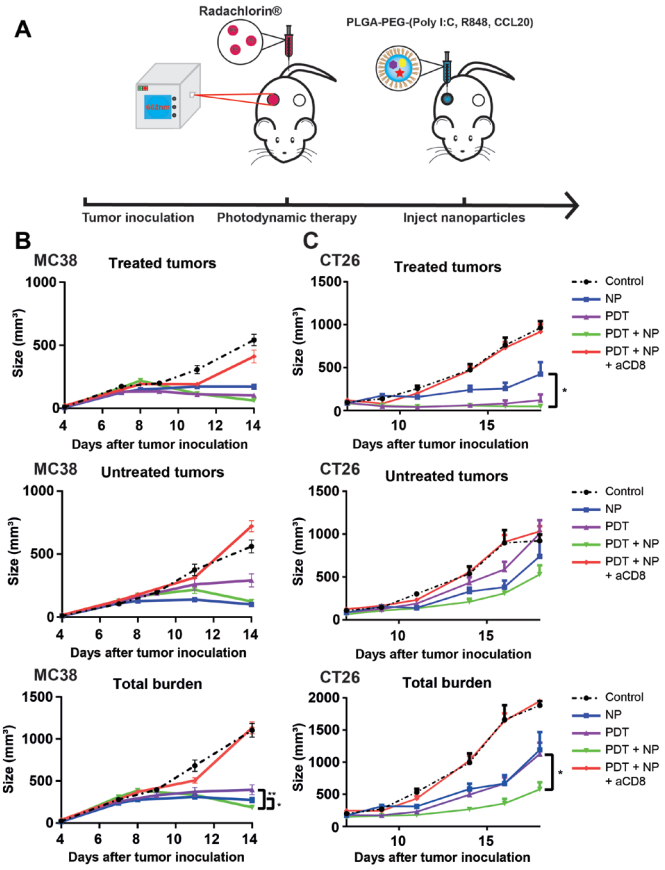

Figure 4. The combination of PDT and NP induces an abscopal effect in mice bearing bilateral MC38 or CT26 tumors.

A). Description of the protocol: immunocompetent mice were inoculated with tumor cells in the right and left flanks (n≥9 mice per group), and injected with CD8-depleting antibodies 1 day before treatment. Once the tumors had become established (~125mm3), the mice were treated with PDT by administering Radachlorin (20 mg/kg) via a tail-vein injection, followed by irradiation (662 nm) at a drug/light interval of 6 h, at 116 mW/cm2 for 116 J/cm2. The next morning, the mice were treated with NPs at an interval of 2 days for a total of four administrations. B). Tumor-growth curves of the treated tumors (upper panel), untreated tumors (middle panel) and total tumor burden (lower panel) for C57BL/6J mice bearing MC38 tumors. C). Tumor-growth curves of the treated tumors (upper panel), untreated tumors (middle panel) and total tumor burden (lower panel) tumors for BALB/c mice bearing CT26 tumors. Statistical analysis was done using the Students t-test, by comparing experimental groups at the indicated timepoints (*p<0.05, **p<0.01 and ***p<0.0001).

The combination of PDT and immunostimulatory NPs provides enhanced tumor-specific immune responses in mice bearing bilateral MC38 or TC-1 tumors

PDT-induced tumor cell death has been suggested to promote the exposure of previously inaccessible (neo)epitopes, which could then trigger tumor-specific immune responses. Accordingly, PDT could simultaneously function both as a direct tumor-killing modality and as an in-situ vaccination strategy. We reasoned that the immunostimulatory effects of PDT might be enhanced through combination with immunostimulatory NPs, which would serve as a potent adjuvant to facilitate tumor-specific T-cell activity. To explore this hypothesis, we inoculated mice with one tumor on each flank, and then treated only one of the tumors with the combination of PDT and NP, as described above (Figure 4A). The day following the second NP administration, the mice were sacrificed and the organs were subsequently collected, and then processed for further analysis. The presence of tumor-specific T cells among splenocytes obtained from these mice was investigated by stimulation with D1 dendritic cells preloaded with the MC38 neoepitopes Adpgk or Rpl1856, and subsequent analysis of intracellular cytokine production. Interestingly, splenocytes from the mice treated with the combination exhibited greater levels of CD8+ T cells positive for IFN γ and TNFα after incubation with Adpgk- (Figure 5A) or Rpl18- (Figure 5B). These results indicate that the combination can enhance specific anti-tumor immune responses, for which the NPs appear to have a stronger effect than PDT. Furthermore, for the TC-1 model, we measured the HPV-E7-specific CD8+ T cells in blood 8 days post-treatment, and observed a considerably higher number of these cells in the animals that had been treated with the combination than in those treated with either single treatments or in the control (untreated) mice (Figure 6C). Together, these results suggest that the combination enhances MC38-neoepitope-specific CD8+ T cells in the spleen and induces high circulating levels of TC-1-specific CD8+ T cells, and that these effects are superior compared to those observed for either PDT or immunostimulatory NPs alone.

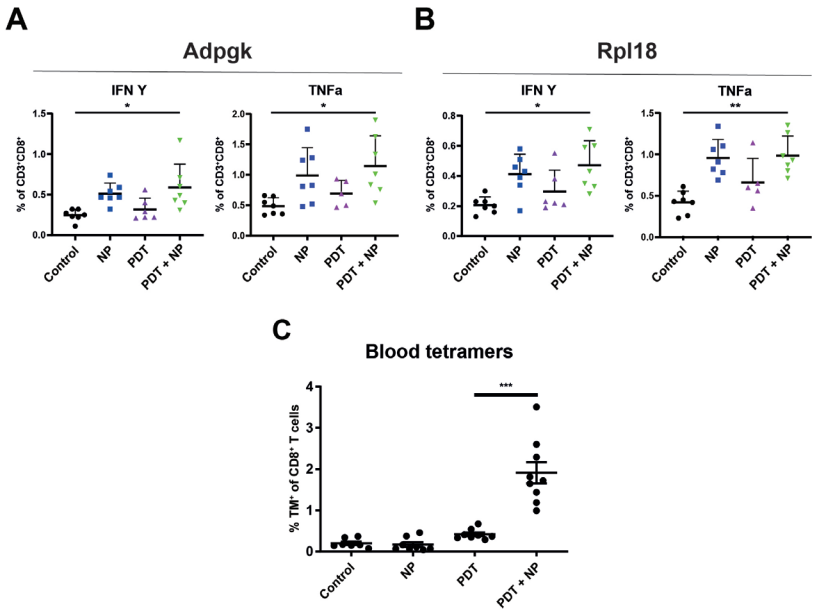

Figure 5. The combination of PDT and immunostimulatory NPs induces enhanced tumor-specific immune responses

Description of the protocol: immunocompetent mice were inoculated with tumor cells in the right and left flanks (n≥5 mice per group), and then injected with CD8-depleting antibodies 1 day before treatment. Once the tumors had become established (~125mm3), the mice were treated with PDT by administering Radachlorin (20 mg/kg) via a tail-vein injection, followed by irradiation (662 nm) at a drug/light interval of 6 h, at 116 mW/cm2 for 116 J/cm2. The next morning, the mice were treated with NPs at an interval of 2 days for a total of two administrations. The day following the second NP administration, the mice were sacrificed, and their spleens were collected and processed for further analysis. Isolated splenocytes were incubated with D1DCs loaded with the MC38 neoepitopes Adpgk (A) or Rpl18 (B) in the presence of Brefeldin A, after which, the CD8+ T cells were analyzed for production of intracellular cytokines. C). Evaluation of tumor-antigen-specific CD8+ T cells in the blood of C57BL/6J mice bearing a single TC-1 tumor at day 8 post-treatment. Tumor-antigen-specific CD8+ T cells were stained with APC-labeled HPV16 E749-57 (RAHYNIVTF) MHC class I (H-2Db) tetramers and then, detected by flow cytometry. Significance was determined using the Mann-Whitney U test (*p<0.01; **p<0.001, ***P<0.0001).

The combination treatment induces an inflammatory state in colon tumors in mice

Having demonstrated that the combination of PDT and immunostimulatory NPs reduced the tumor burden of colon cancers in vivo in a CD8+ T cell-dependent manner, we further investigated the anti-tumor immune response elicited by this treatment, by analyzing diverse immune cell populations present in the tumor microenvironment and secondary lymphoid organs. To this end, we inoculated mice with two MC38 or two CT26 tumors, one on each flank, and then treated only one tumor with the combination, as described above (Figure 4A). The day following the second NP administration, the mice were sacrificed, and several of their several organs were collected and prepared for analysis by flow cytometry. In the MC38 model, all treatments induced the infiltration of neutrophils in the treated tumor (Figure 6A), as previously described for PDT.57 Interestingly, NPs also induced infiltration of neutrophils in the untreated tumor (Figure S4A). The levels of mature (CD86+) and inflammatory (Ly6Chigh) myeloid cells have recently been shown to increase in treatment-responsive tumors but not in relapsed tumors that display resistance to treatment.58 In line with this, we observed an increase in the levels of mature inflammatory myeloid cells and a decrease in non-inflammatory (Ly6C-) cells in the treated tumor after treatment with the combination compared to all other treatments (Figure 6A). In the untreated tumor, the levels of mature inflammatory monocytes were slightly decreased while the non-inflammatory myeloid cells were increased (Figure S4A). These data indicate the ability of the combination to increase mature inflammatory myeloid cells in the treated tumor, but not in the untreated tumor, which in turn is reflected by the responsiveness to treatment. In the dLN of MC38 tumor-bearing mice, the NP and combination treatments led to increased populations of CD11b+ and DC (Figure S4A). In the spleen, the CD11b+ population was also increased whereas the DC population wase decreased after the combination treatment (Figure S4A). In both the dLN and the spleen, the number of CD4+ T cells were decreased whereas the CD8+ T cells were increased (Figure S4A). These results indicate that CD11b+ cells, including antigen-presenting cells, are increased in the dLN of treated mice, while the CD4+/CD8+ T-cell ratio is skewed to favor CD8+ T cells in the dLN and spleen, which corroborate the tumor-specific, CD8+ T-cell responses that we previously found to be essential for efficacy. We observed a similar trend in the CT26 tumor-bearing mice, in which the combination treatment increased the levels of neutrophils in the

treated tumor (Figure 6B) and, to a lesser extent, in the untreated tumor (Figure S4B). Furthermore, the combination increased the number of mature inflammatory myeloid cells and decreased the non-inflammatory cells, in both the treated and the untreated tumors. In the dLN and spleens of the CT26 tumor-bearing mice, the combination induced a strong increase in the number of CD11b+ cells and DCs (Figure S4B). In the dLN, the CD4+/CD8+ T-cell ratio was similar among all treatments (Figure S4B); however, in the spleen, the NP and combination treatments shifted this ratio to CD8+ T cells, albeit marginally (Figure S4B). Together, these data indicate that in tumor-bearing mice, the combination of PDT and immunostimulatory NPs induces inflammation in the tumor microenvironment, coinciding with greater neutrophil infiltration, and higher levels of CD11b+ cells and DCs in secondary lymphoid organs. Moreover, this combination appears to skew the CD4+/CD8+ T-cell ratio in favor of CD8+ T cells, in line with our previous observation that the efficacy of this combination is dependent on tumor-specific CD8+ T cells.

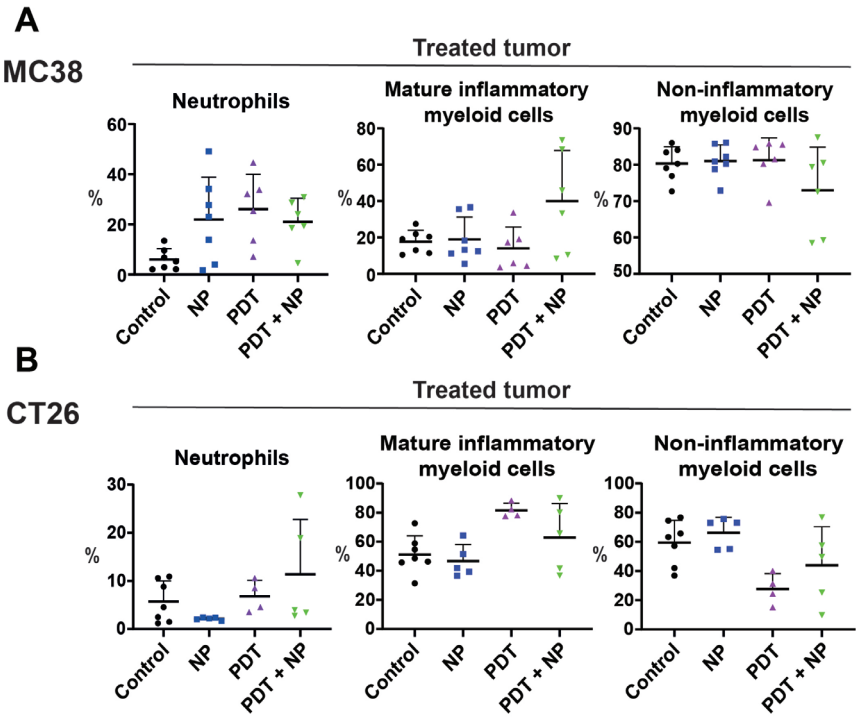

Figure 6. The combination of PDT and immunostimulatory NPs induces an inflammatory state in the tumor microenvironment

Immunocompetent mice were inoculated with bilateral MC38 or CT26 tumors (n≥5 mice), in the right and left flanks (n≥5 mice per group). Once the tumors had become established (~125mm3), the mice were treated with PDT by administering Radachlorin (20 mg/kg) via a tail-vein injection, followed by irradiation (662 nm) at a drug/light interval of 6 h, at 116 mW/cm2 for 116 J/cm2. The next morning, the mice were treated with the immunostimulatory NPs at an interval of 2 days for a total of two administrations. The day following the second NP administration, the mice were sacrificed, after which the tumors were collected, processed, and stained for analysis by flow cytometry. Cell populations are shown in percentages for mice bearing bilateral MC38 (A) or CT26 (B) tumors. Gating was performed in FlowJo and included only living (7AAD-) CD45.2+ cells. Populations were further gated to include neutrophils (CD11b+Ly6G+), mature inflammatory myeloid cells (CD11b+CD86+Ly6Chi) and non-inflammatory myeloid cells (CD11b+Ly6Clow).

DISCUSSION

The tumor debulking effects of photodynamic therapy are often insufficient to induce complete and lasting therapeutic efficacy. However, recent studies that exploit the ability of PDT to initiate immune responses in combination with immunotherapy show great promise.59–61 In the present study, we combined PDT with immunostimulatory NPs loaded with poly(I:C), R848 and MIP3α. We synthesized these biodegradable PLGA NPs, loaded them with immunostimulatory agents, and characterized them, finding favorable physicochemical properties, a lack of inherent cytotoxicity, and retention of biological activities of the encapsulated immunostimulatory agents. Consistent with literature reports on the immunostimulatory activities of PDT on myeloid cells,4,14,62–66 in our studies, PDT-induced tumor cell death led to the upregulation of dendritic cell maturation markers in vitro.

Expanding on our in vitro findings, we explored our therapeutic combination in mice bearing a single tumor. All treatments fully eradicated the MC38 tumors, extended the survival of MC38-tumor-bearing mice and were highly effective in delaying the growth of CT26 tumors, with the combination being significantly more effective against CT26 than either treatment alone. TC-1 tumors were less responsive to all treatments, with the combination strongly inhibiting tumor growth compared to either treatment alone in addition to the control, but not inducing significant gains in survival. Our therapeutic combination performs well compared to similar strategies that use PDT and immunostimulatory agents. It shows an efficacy equal to or better than PDT combined with photo-thermal therapy (PTT) and TLR9-agonist CpG,65 PDT combined with CpG and a hypoxia inducible factor (HIF) inhibitor,64 CD276-targeted PDT combined with immune checkpoint inhibitors,67 and PDT with magnetic hyperthermia and immune checkpoint inhibitors,68 that all show a tumor growth inhibition at early timepoints after treatment, but do not show long term survival (up to 50 days). The differences in response to PDT-treatment in vivo among the tumor models is further reflected by our observation of upregulation of DC maturation markers in the PDT-treated tumor cells in vitro, whereby MC38 cells exhibited the greatest upregulation of maturation markers, followed by CT26, while TC-1 cells showed only a slight upregulation. These results suggest a link between the propensity of dying PDT-treated tumor cells to upregulate DC maturation markers and the anti-tumor efficacy of PDT.

In the in vivo experiments exploring bilateral tumors, the PDT-nanoparticle combination most effectively reduced the total tumor burden compared to either treatment alone. The efficacy of our combination is comparable to a study combining PDT with PTT,69 and a study combining PDT with PTT and an indoleamine 2,3-dioxygenase inhibitor.66 However, studies that combine PDT with immune checkpoint inhibitors often show improved results, mostly on the untreated (distal) tumors.59–61 Importantly, in both the unilateral and the bilateral tumor models, pre-treatment depletion of CD8+ cells abrogated the efficacy of the combination treatment. This observation is in line with previously published results,17 and confirms the importance of CD8+ cells to the benefits of this treatment. Furthermore, the ability of the treatment to induce tumor-specific immune responses was investigated by stimulating the splenocytes of treated, tumor-bearing mice ex vivo with the MC38 neoepitopes Adpgk and Rpl18. This revealed an expansion of these tumor-specific CD8+ T cells producing the cytokines IFN-γ and TNF-α in the treated mice compared to control (untreated) mice, in which the NPs played the largest role (Fig 5). Additionally, the combination induced significantly higher levels of tumor specific CD8+ T cells to TC-1 tumors compared to either treatment alone. These observations corroborate literature that describes PDT as a modality that facilitates the exposure of previously inaccessible tumor epitopes to induce and/or enhance tumor-specific immune responses. This ability of PDT to function as an in situ vaccination modality has often been hypothesized, however, it has to our knowledge only been shown for exogenous antigens (ovalbumin),70 and not for cancer neoepitopes (Rpl18 and Adpgk). Although high levels of circulating tumor-specific T cells to TC-1 (HPV16 E7) have been shown after combining PDT with specific vaccination using synthetic long peptides for TC-1,54 we report strongly elevated blood levels of such T cells after combination with nonspecific immunostimulatory NPs, thereby providing proof to the in situ vaccination ability of PDT when it is combined with a strong adjuvant.

Finally, we evaluated the immunological composition of the tumor microenvironment after treatment of tumor-bearing mice. Our data show that the combination treatment alters the immunosuppressive tumor microenvironment into a more proinflammatory one, by increasing the presence of mature inflammatory myeloid cells and decreasing the non-inflammatory monocytes in the treated tumor. This observation is in line with other studies combining PDT and immunotherapy that also show an increased inflammatory state in the tumor after treatment.61,64–66,68,71 Immune

checkpoint inhibitors have been shown to enhance the infiltration of CD8+ T cells in the untreated (distal) tumor, whereas PDT alone did not.59,60 Our observations that local treatment with immune stimulating nanoparticles combined with PDT induces a potent tumor-specific CD8+ T cell response, provides a rationale for further enhancing abscopal effects by systemic treatment with immune checkpoint inhibitors. Clinical efficacy of immune checkpoint inhibitors is often hampered by the immunosuppressive state present in the tumor microenvironment,72 which we may repolarize to more proinflammatory after our local nanoparticle treatment. In practice, also intravenous injection may result in accumulation of the immunostimulatory NP in untreated (distal) tumors. Therefore, a protocol that combines PDT with intravenously administered PLGA-PEG(poly(I:C), R848, MIP-3α) and immune checkpoint inhibitors could be of clinical advantage. Our future studies will explore the potential of such protocols in the treatment of primary and metastatic tumors.

Together, our results show that the combination of PDT and immunostimulatory NPs functions as an in situ vaccination strategy that induces strong, CD8+ T cell-dependent, anti-tumor immune responses and elicits abscopal effects. As the benefits of combining classical ablation and immune therapies treatments are increasingly appreciated,73–75 the potential of our PDT-nanoparticle combination that we have presented in this study may contribute to more effective treatment protocols for solid tumors.

REFERENCES

1. van Straten D, Mashayekhi V, de Bruijn HS, Oliveira S, Robinson DJ. Oncologic photodynamic therapy: Basic principles, current clinical status and future directions. Cancers (Basel). 2017;9(2). doi:10.3390/cancers9020019
2. Beltrán Hernández I, Yu Y, Ossendorp F, Korbelik M, Oliveira S. Preclinical and Clinical Evidence of Immune Responses Triggered in Oncologic Photodynamic Therapy: Clinical Recommendations. J Clin Med. 2020;9(2):333. doi:10.3390/jcm9020333
3. Nath S, Obaid G, Hasan T. The Course of Immune Stimulation by Photodynamic Therapy: Bridging Fundamentals of Photochemically Induced Immunogenic Cell Death to the Enrichment of T-Cell Repertoire. Photochem Photobiol. 2019;95(6):1288-1305. doi:10.1111/php.13173
4. Li W, Yang J, Luo L, et al. Targeting photodynamic and photothermal therapy to the endoplasmic reticulum enhances immunogenic cancer cell death. Nat Commun. 2019;10(1):3349. doi:10.1038/s41467-019-11269-8
5. Scaffidi P, Misteli T, Bianchi ME. Release of chromatin protein HMGB1 by necrotic cells triggers inflammation. Nature. 2002;418(6894):191-195. doi:10.1038/nature00858
6. Obeid M, Tesniere A, Ghiringhelli F, et al. Calreticulin exposure dictates the immunogenicity of cancer cell death. Nat Med. 2007;13(1):54-61. doi:10.1038/nm1523
7. Obeid M, Tesniere A, Panaretakis T, et al. Ecto-calreticulin in immunogenic chemotherapy. Immunol Rev. 2007;220(1):22-34. doi:10.1111/j.1600-065X.2007.00567.x
8. Korbelik M, Sun J, Cecic I. Photodynamic Therapy − Induced Cell Surface Expression and Release of Heat Shock Proteins : Relevance for Tumor Response. Cancer Res. 2005;65(3):1018-1026.
9. Krysko D V, Garg AD, Kaczmarek A, Krysko O, Agostinis P, Vandenabeele P. Immunogenic cell death and DAMPs in cancer therapy. Nat Rev Cancer. 2012;12. doi:10.1038/nrc3380
10. Panzarini E, Inguscio V, Fimia GM, Dini L. Rose Bengal Acetate PhotoDynamic Therapy (RBAc-PDT) Induces Exposure and Release of Damage-Associated Molecular Patterns (DAMPs) in Human HeLa Cells. 2014. doi:10.1371/journal.pone.0105778
11. Vabulas RM, Wagner H, Schild H. Heat shock proteins as ligands of Toll-like receptors. Curr Top Microbiol Immunol. 2002;270:169-184. doi:10.1007/978-3-642-59430-4_11

12. Jessica B. Flechtner, Kenya Prince Cohane, Sunil Mehta, Paul Slusarewicz, Alexis Kays Leonard BHB, Andjelic DLL and S. High-Affinity Interactions between Peptides and Heat Shock Protein 70 Augment CD8+ T Lymphocyte Immune Responses. J Immunol. 2006;(177):1017-1027. doi:10.4049/jimmunol.177.2.1017
13. Salimu J, Spary LK, Al-Taei S, et al. Cross-Presentation of the Oncofetal Tumor Antigen 5T4 from Irradiated Prostate Cancer Cells--A Key Role for Heat-Shock Protein 70 and Receptor CD91. Cancer Immunol Res. 2015;3(6):678-688. doi:10.1158/2326-6066.CIR-14-0079
14. Garg AD, Krysko D V, Verfaillie T, et al. A novel pathway combining calreticulin exposure and ATP secretion in immunogenic cancer cell death. EMBO J. 2012;31(5):1062-1079. doi:10.1038/emboj.2011.497
15. Elliott MR, Chekeni FB, Trampont PC, et al. Nucleotides released by apoptotic cells act as a find-me signal to promote phagocytic clearance. Nature. 2009;461(7261):282-286. doi:10.1038/nature08296
16. Ghiringhelli F, Apetoh L, Tesniere A, et al. Activation of the NLRP3 inflammasome in dendritic cells induces IL-1β–dependent adaptive immunity against tumors. Nat Med. 2009;15(10):1170-1178. doi:10.1038/nm.2028
17. Kleinovink JW, Fransen MF, Löwik CW, Ossendorp F. Photodynamic-Immune Checkpoint Therapy Eradicates Local and Distant Tumors by CD8(+) T Cells. Cancer Immunol Res. 2017;5(10):832-838. doi:10.1158/2326-6066.CIR-17-0055
18. Maria Theophiel Van Nuffel A, Garg AD, Leuven K, et al. Immunomodulation of the Tumor Microenvironment: Turn Foe Into Friend. Front Immunol | www.frontiersin.org. 2018;9:2909. doi:10.3389/fimmu.2018.02909
19. Da Silva CG, Camps MGM, Li TMWY, Zerrillo L, Löwik CW, Cruz LJ. Effective chemoimmunotherapy by co-delivery of doxorubicin and immune adjuvants in biodegradable nanoparticles. Theranostics. 2019;9:22. doi:10.7150/thno.34429
20. Da Silva CG, Camps MGM, Li TMWY, Chan AB, Ossendorp F, Cruz LJ. Co-delivery of immunomodulators in biodegradable nanoparticles improves therapeutic efficacy of cancer vaccines. Biomaterials. 2019;220. doi:10.1016/j.biomaterials.2019.119417
21. Smith M, García-Martínez E, Pitter MR, et al. Trial Watch: Toll-like receptor agonists in cancer immunotherapy. 2018. doi:10.1080/2162402X.2018.1526250
22. Cheng Y-S, Xu F. Anticancer function of polyinosinic-polycytidylic acid. Cancer Biol Ther 1219 Cancer Biol Ther. 2010;10:1219-1223. doi:10.4161/cbt.10.12.13450

23. Shime H, Matsumoto M, Seya T. Double-stranded RNA promotes CTL-independent tumor cytolysis mediated by CD11b+Ly6G+ intratumor myeloid cells through the TICAM-1 signaling pathway. Cell Death Differ. 2017;24:385-396. doi:10.1038/cdd.2016.131
24. Shime H, Matsumoto M, Oshiumi H, et al. Toll-like receptor 3 signaling converts tumor-supporting myeloid cells to tumoricidal effectors. doi:10.1073/pnas.1113099109
25. Takemura R, Takaki H, Okada S, et al. PolyI:C-Induced, TLR3/RIP3-Dependent Necroptosis Backs Up Immune Effector-Mediated Tumor Elimination In Vivo. Cancer Immunol Res. 2015;3(8):902-914. doi:10.1158/2326-6066.CIR-14-0219
26. Salmon H, Idoyaga J, Rahman A, et al. Expansion and activation of CD103 + dendritic cell progenitors at the tumor site enhances tumor responses to therapeutic PD-L1 and BRAF inhibition HHS Public Access. Immunity. 2016;44(4):924-938. doi:10.1016/j.immuni.2016.03.012
27. Friboulet L, Pioche-Durieu C, Rodriguez S, et al. Recurrent Overexpression of c-IAP2 in EBV-Associated Nasopharyngeal Carcinomas: Critical Role in Resistance to Toll-like Receptor 3-Mediated Apoptosis 1,2. 2008;10:1183. doi:10.1593/neo.08590
28. Paone A, Starace D, Galli R, et al. Toll-like receptor 3 triggers apoptosis of human prostate cancer cells through a PKC-a-dependent mechanism. Carcinogenesis. 2008;29(7):1334-1342. doi:10.1093/carcin/bgn149
29. Weber A, Kirejczyk Z, Besch R, Potthoff S, Leverkus M, Häcker G. Proapoptotic signalling through Toll-like receptor-3 involves TRIF-dependent activation of caspase-8 and is under the control of inhibitor of apoptosis proteins in melanoma cells. 2010. doi:10.1038/cdd.2009.190
30. Estornes Y, Toscano F, Virard F, et al. dsRNA induces apoptosis through an atypical death complex associating TLR3 to caspase-8. Cell Death Differ. 2012;19:1482-1494. doi:10.1038/cdd.2012.22
31. Zhou Z, Sun L. Immune effects of R848: Evidences that suggest an essential role of TLR7/8-induced, Myd88- and NF-κB-dependent signaling in the antiviral immunity of Japanese flounder (Paralichthys olivaceus). Dev Comp Immunol. 2015;49(1):113-120. doi:10.1016/j.dci.2014.11.018
32. YIN T, HE S, WANG Y. Toll-like receptor 7/8 agonist, R848, exhibits antitumoral effects in a breast cancer model. Mol Med Rep. 2015;12(3):3515-3520. doi:10.3892/mmr.2015.3885

33. Spinetti T, Spagnuolo L, Mottas I, et al. TLR7-based cancer immunotherapy decreases intratumoral myeloid-derived suppressor cells and blocks their immunosuppressive function. Oncoimmunology. 2016;5(11):e1230578. doi:10.1080/2162402X.2016.1230578
34. Rodell CB, Arlauckas SP, Cuccarese MF, et al. TLR7/8-agonist-loaded nanoparticles promote the polarization of tumour-associated macrophages to enhance cancer immunotherapy. Nat Biomed Eng. 2018;2:578-588. http://www.ncbi.nlm.nih.gov/pubmed/30345161. Accessed April 30, 2019.
35. Ye J, Ma C, Hsueh EC, et al. TLR8 signaling enhances tumor immunity by preventing tumor-induced T-cell senescence. doi:10.15252/emmm.201403918
36. Hieshima K, Imai T, Opdenakker G, et al. Molecular cloning of a novel human CC chemokine liver and activation-regulated chemokine (LARC) expressed in liver. Chemotactic activity for lymphocytes and gene localization on chromosome 2. J Biol Chem. 1997;272(9):5846-5853. doi:10.1074/jbc.272.9.5846
37. Mclean MH, Murray GI, Stewart KN, et al. The Inflammatory Microenvironment in Colorectal Neoplasia. doi:10.1371/journal.pone.0015366
38. Frick VO, Rubie C, Keilholz U, Ghadjar P. Chemokine/chemokine receptor pair CCL20/CCR6 in human colorectal malignancy: An overview. World J Gastroenterol. 2016;22(2):833-841. doi:10.3748/wjg.v22.i2.833
39. Kwong B, Liu H, Irvine DJ. Induction of potent anti-tumor responses while eliminating systemic side effects via liposome-anchored combinatorial immunotherapy. Biomaterials. 2011;32(22):5134-5147. doi:10.1016/j.biomaterials.2011.03.067
40. Da Silva CG, Rueda F, Löwik CW, Ossendorp F, Cruz LJ. Combinatorial prospects of nano-targeted chemoimmunotherapy. Biomaterials. 2016;83:308-320. doi:10.1016/J.BIOMATERIALS.2016.01.006
41. Makadia HK, Siegel SJ. Poly Lactic-co-Glycolic Acid (PLGA) as Biodegradable Controlled Drug Delivery Carrier. Polymers (Basel). 2011;3(3):1377-1397. doi:10.3390/polym3031377
42. LaVan DA, McGuire T, Langer R. Small-scale systems for in vivo drug delivery. Nat Biotechnol. 2003;21(10):1184-1191. doi:10.1038/nbt876
43. Huis in 't Veld R V., Ritsma L, Kleinovink JW, Que I, Ossendorp F, Cruz LJ. Photodynamic cancer therapy enhances accumulation of nanoparticles in tumor-associated myeloid cells. J Control Release. 2020;320:19-31. doi:10.1016/j.jconrel.2019.12.052

44. Barr H, Krasner N, Boulos PB, Chatlani P, Bown SG. Photodynamic therapy for colorectal cancer: A quantitative pilot study. Br J Surg. 1990;77(1):93-96. doi:10.1002/bjs.1800770132
45. McCaughan JS, Hawley PC, Bethel BH, Walker J. Photodynamic therapy of endobronchial malignancies. Cancer. 1988;62(4):691-701. doi:10.1002/1097-0142(19880815)62:4<691::AID-CNCR2820620408>3.0.CO;2-I
46. Cruz LJ, Tacken PJ, Fokkink R, et al. Targeted PLGA nano- but not microparticles specifically deliver antigen to human dendritic cells via DC-SIGN in vitro. J Control Release. 2010;144(2):118-126. doi:10.1016/j.jconrel.2010.02.013
47. Cruz LJ, Tacken PJ, Bonetto F, et al. Multimodal Imaging of Nanovaccine Carriers Targeted to Human Dendritic Cells. Mol Pharm. 2011;8(2):520-531. doi:10.1021/mp100356k
48. Cruz LJ, Tacken PJ, Rueda F, Domingo JC, Albericio F, Figdor CG. Targeting Nanoparticles to Dendritic Cells for Immunotherapy. Methods Enzymol. 2012;509:143-163. doi:10.1016/B978-0-12-391858-1.00008-3
49. Cruz LJ, Stammes MA, Que I, et al. Effect of PLGA NP size on efficiency to target traumatic brain injury. J Control Release. 2016;223:31-41. doi:10.1016/J.JCONREL.2015.12.029
50. Tel J, Lambeck AJA, Cruz LJ, Tacken PJ, de Vries IJM, Figdor CG. Human Plasmacytoid Dendritic Cells Phagocytose, Process, and Present Exogenous Particulate Antigen. J Immunol. 2010;184(8):4276-4283. doi:10.4049/jimmunol.0903286
51. Lin K-Y, Guarnieri FG, Staveley-O'Carroll KF, et al. Treatment of Established Tumors with a Novel Vaccine That Enhances Major Histocompatibility Class II Presentation of Tumor Antigen. Cancer Res. 1996;56(1).
52. Ossendorp F, Fu N, Camps M, et al. Differential Expression Regulation of the α and β Subunits of the PA28 Proteasome Activator in Mature Dendritic Cells. J Immunol. 2005;174(12):7815-7822. doi:10.4049/jimmunol.174.12.7815
53. Zom GG, Khan S, Britten CM, et al. Efficient induction of antitumor immunity by synthetic toll-like receptor ligand-peptide conjugates. Cancer Immunol Res. 2014;2(8):756-764. doi:10.1158/2326-6066.CIR-13-0223
54. Kleinovink JW, van Driel PB, Snoeks TJA, et al. Combination of photodynamic therapy and specific immunotherapy efficiently eradicates established tumors. Clin Cancer Res. 2015. doi:10.1158/1078-0432.CCR-15-0515

55. Yadav M, Jhunjhunwala S, Phung QT, et al. Predicting immunogenic tumour mutations by combining mass spectrometry and exome sequencing. Nature. 2014;515(7528):572-576. doi:10.1038/nature14001
56. Hos BJ, Camps MGM, Bulk J van den, et al. Identification of a neo-epitope dominating endogenous CD8 T cell responses to MC-38 colorectal cancer. Oncoimmunology. 2020;9(1). doi:10.1080/2162402X.2019.1673125
57. Cecic I, Parkins CS, Korbelik M. Induction of Systemic Neutrophil Response in Mice by Photodynamic Therapy of Solid Tumors¶. Photochem Photobiol. 2001;74(5):712. doi:10.1562/0031-8655(2001)074<0712:iosnri>2.0.co;2
58. Beyranvand Nejad E, Labrie C, Abdulrahman Z, et al. Lack of myeloid cell infiltration as an acquired resistance strategy to immunotherapy. J Immunother Cancer. 2020;8(2):1326. doi:10.1136/jitc-2020-001326
59. Xu J, Xu L, Wang C, et al. Near-Infrared-Triggered Photodynamic Therapy with Multitasking Upconversion Nanoparticles in Combination with Checkpoint Blockade for Immunotherapy of Colorectal Cancer. doi:10.1021/acsnano.7b00715
60. He C, Duan X, Guo N, et al. Core-shell nanoscale coordination polymers combine chemotherapy and photodynamic therapy to potentiate checkpoint blockade cancer immunotherapy. Nat Commun. 2016;7(1):12499. doi:10.1038/ncomms12499
61. Zhou Y, Liu S, Hu C, Cai L, Pang M. A covalent organic framework as a nanocarrier for synergistic phototherapy and immunotherapy †. J Mater Chem B. 2020;8:5451. doi:10.1039/d0tb00679c
62. Ji J, Fan Z, Zhou F, et al. Improvement of DC vaccine with ALA-PDT induced immunogenic apoptotic cells for skin squamous cell carcinoma. 2015;6(19):17135-17146.
63. Jung N, Jung H, Kang M, et al. Photodynamic therapy-mediated DC immunotherapy is highly effective for the inhibition of established solid tumors. 2012;324:58-65.
64. Cai Z, Xin F, Wei Z, et al. Photodynamic Therapy Combined with Antihypoxic Signaling and CpG Adjuvant as an In Situ Tumor Vaccine Based on Metal–Organic Framework Nanoparticles to Boost Cancer Immunotherapy. Adv Healthc Mater. 2020;9(1):1900996. doi:10.1002/adhm.201900996
65. Chen L, Zhou L, Wang C, et al. Tumor-Targeted Drug and CpG Delivery System for Phototherapy and Docetaxel-Enhanced Immunotherapy with Polarization toward M1-Type Macrophages on Triple Negative Breast Cancers. Adv Mater. 2019;31(52):1904997. doi:10.1002/adma.201904997

66. Yang W, Zhang F, Deng H, et al. Smart Nanovesicle-Mediated Immunogenic Cell Death through Tumor Microenvironment Modulation for Effective Photodynamic Immunotherapy. ACS Nano. 2020;14(1):620-631. doi:10.1021/acsnano.9b07212
67. Bao R, Wang Y, Lai J, et al. Enhancing Anti-PD-1/PD-L1 Immune Checkpoint Inhibitory Cancer Therapy by CD276-Targeted Photodynamic Ablation of Tumor Cells and Tumor Vasculature. Mol Pharm. November 2018:acs.molpharmaceut.8b00997. doi:10.1021/acs.molpharmaceut.8b00997
68. Wang Z, Zhang F, Shao D, et al. Janus Nanobullets Combine Photodynamic Therapy and Magnetic Hyperthermia to Potentiate Synergetic Anti-Metastatic Immunotherapy. Adv Sci. 2019;6(22). doi:10.1002/advs.201901690
69. Yang J, Hou M, Sun W, et al. Sequential PDT and PTT Using Dual-Modal Single-Walled Carbon Nanohorns Synergistically Promote Systemic Immune Responses against Tumor Metastasis and Relapse. Adv Sci. 2020;7(16). doi:10.1002/advs.202001088
70. Yang W, Zhu G, Wang S, et al. In Situ Dendritic Cell Vaccine for Effective Cancer Immunotherapy. ACS Nano. 2019;13(3):3083-3094. doi:10.1021/acsnano.8b08346
71. Wu X, Yang H, Chen X, et al. Nano-herb medicine and PDT i nduced synergistic immunotherapy for colon cancer treatment. Biomaterials. 2021;269:120654. doi:10.1016/j.biomaterials.2021.120654
72. Jenkins RW, Barbie DA, Flaherty KT. Mechanisms of resistance to immune checkpoint inhibitors. Br J Cancer. 2018;118(1):9-16. doi:10.1038/bjc.2017.434
73. Lopez JS, Banerji U. Combine and conquer: challenges for targeted therapy combinations in early phase trials. Nat Rev Clin Oncol. 2017;14(1):57-66. doi:10.1038/nrclinonc.2016.96
74. Mahoney KM, Rennert PD, Freeman GJ. Combination cancer immunotherapy and new immunomodulatory targets. Nat Rev Drug Discov. 2015;14(8):561-584. doi:10.1038/nrd4591
75. Gotwals P, Cameron S, Cipolletta D, et al. Prospects for combining targeted and conventional cancer therapy with immunotherapy. Nat Rev Cancer. 2017;17(5):286-301. doi:10.1038/nrc.2017.17

COMBINING PHOTODYNAMIC THERAPY WITH IMMUNOSTIMULATORY NANOPARTICLES ELICITS EFFECTIVE ANTI-TUMOR IMMUNE RESPONSES IN PRECLINICAL MURINE MODELS

Huis in 't Veld, Ruben V.; da Silva, Candido G.; Jager, Martine J.; Cruz, Luis J.; Ossendorp, Ferry.

Supplementary Figures

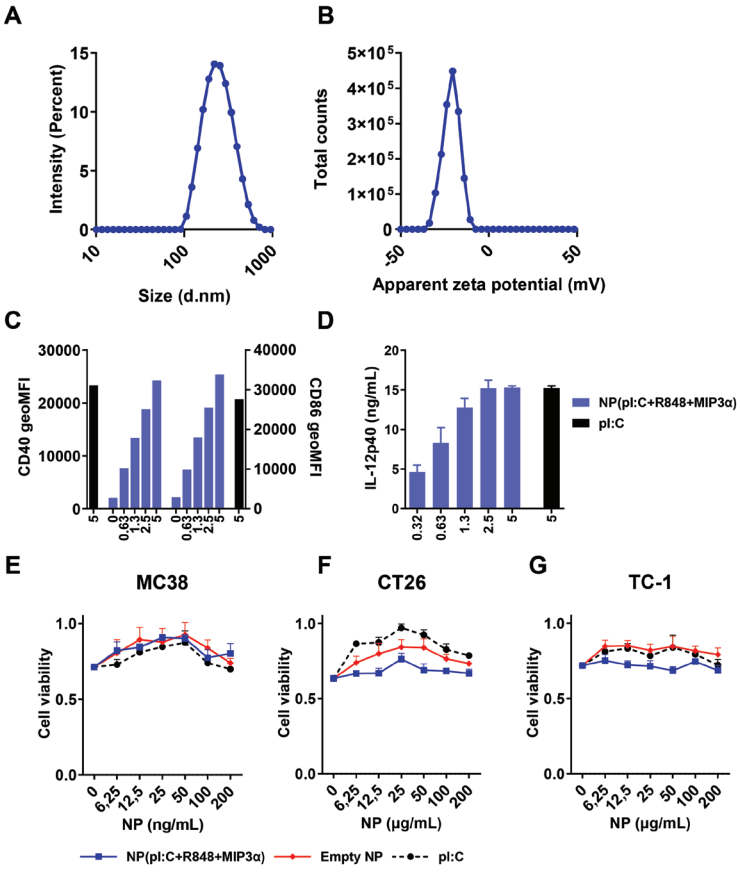

Figure S1. Synthesis and characterization of PLGA-PEG(poly(I:C), R848, MIP-3α)

A). Size distribution and B). distribution of the ζ-potential of the PLGA-PEG-NPs used in this study. C). Maturation of D1DCs after 24 h of incubation with the NP added to correspond to concentrations of 0-5 μg/mL poly(I:C) (light blue bars) compared to 5 μg/mL pure poly(I:C) (black bars), shown as expression of CD40 (left bars) and CD86 (right bars). D). IL-12P40 expression by D1DCs after 24 h of incubation with the NP at indicated concentration (light blue bars) compared to 5 μg/mL pure poly(I:C) (black bars). E-G). Toxicity of the NPs to MC38, CT26 and TC-1 after 72 h of incubation at indicated concentrations compared to free poly(I:C) and empty NPs incubated at equal concentrations, determined using the MTS assay.

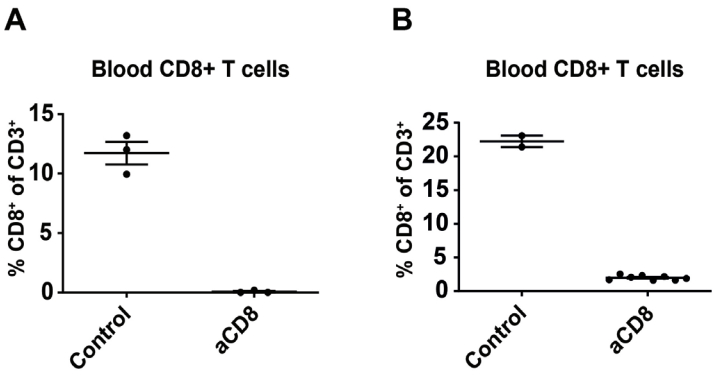

Figure S2. Blood levels of CD8+ cells after treatment with CD8-depleting antibodies

Levels of CD8+ cells in blood of mice bearing a single MC38 (A) or CT26 (B) tumor in control (untreated) mice and mice that received CD8-depleting antibodies (aCD8), measured 1 day after administering CD8-depleting antibodies.

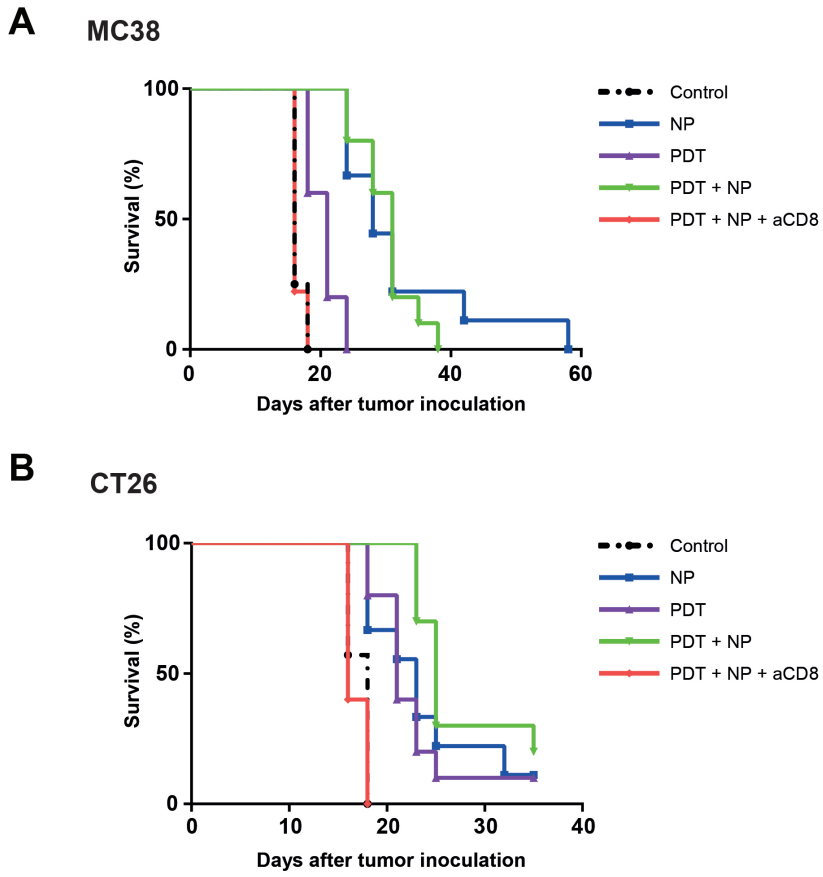

Figure S3. Survival curves of mice bearing bilateral MC38 or CT26 tumors

Immunocompetent mice were inoculated with tumor cells in the right and left flanks and injected with CD8-depleting antibodies one day before tumors became established. When the tumors were established (~125mm3), PDT was performed on one tumor by administration of 20 mg/kg Radachlorin in the tail vein and irradiating with 662 nm light at a drug-to light interval of 6h and 116 mW/cm2 for 116 J/cm2. The next morning, animals were injected with NPs at an interval of 2 days for a total of 4 administrations. Survival curves of mice bearing two A). MC38 tumors (C57BL/6J mice) and B). CT26 tumors (BALB/c mice), one on each opposite flank.

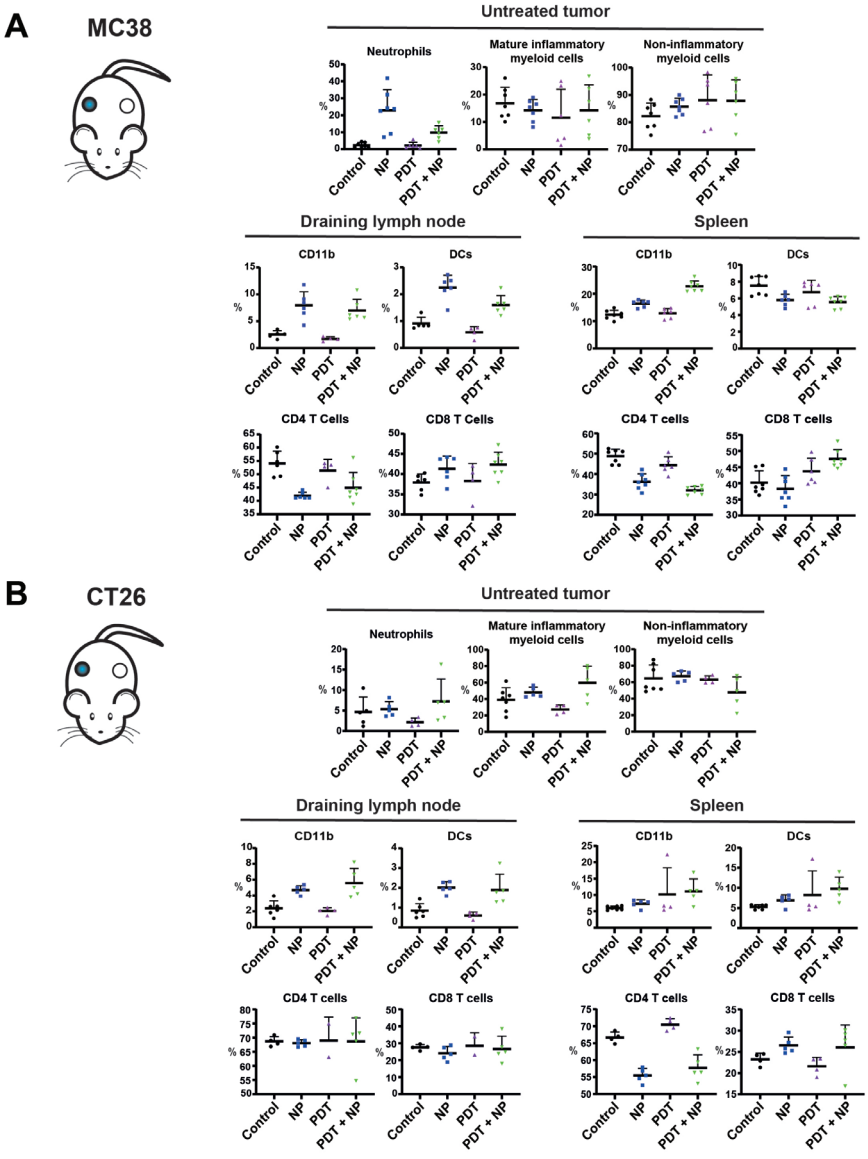
A
MC38
Untreated tumor
Neutrophils
Mature inflammatory myeloid cells
Non-inflammatory myeloid cells
Draining lymph node
Spleen
CD11b
DCs
CD4 T Cells
CD8 T Cells
CD4 T cells
CD8 T cells
Control
NP
PDT
PDT + NP
B
CT26
Untreated tumor
Neutrophils
Mature inflammatory myeloid cells
Non-inflammatory myeloid cells
Draining lymph node
Spleen
CD11b
DCs
CD4 T cells
CD8 T cells
Control
NP
PDT
PDT + NP

Figure S4. Analysis of the tumor microenvironment after treatment

Immunocompetent mice were inoculated with cancer cells in the right and left flanks (n≥5). When the tumors were established (~125mm3), PDT was performed on one tumor by administration of 20 mg/kg Radachlorin in the tail vein and irradiating with 662 nm light at a drug-to light interval of 6h and 116 mW/cm2 for 116 J/cm2. The next morning, animals were injected with NPs at an interval of 2 days for a total of 2 administrations. The day following the second NP administration, the mice were sacrificed after which the dLN and spleen were collected, processed, and stained for analysis by flow cytometry. Populations are shown in percentages for A). MC38 and B). CT26 tumor-bearing mice. Gating was performed in FlowJo and included only living (7AAD-) CD45.2+ cells. Populations were further gated to include neutrophils (CD11b+Ly6G+), mature inflammatory myeloid cells (CD11b+CD86+Ly6Chi), non-inflammatory myeloid cells (CD11b+Ly6Clow), CD11b (total CD11b+), dendritic cells (DCs, CD11b+CD11chi), CD4 T cells (CD3+CD4+) and CD8 T cells (CD3+CD8+).